Final Accepted Version
Published Version at: Whiteman, M.L., Phillips, B.M., Fernández-Cabán, P.L., Masters, F.J., Bridge, J.A., and Davis, J.R. (2018). "Optimal Design of Structures using Cyber-physical Wind Tunnel Experiments with Mechatronic Models." Journal of Wind Engineering and Industrial Aerodynamics, 172. DOI: 10.1016/j.jweia.2017.11.013.

Optimal design of structures using cyber-physical wind tunnel experiments with mechatronic models

Michael L. Whiteman [a], Brian M. Phillips [b*], Pedro L. Fernández Cabán [c], Forrest J. Masters [d], Jennifer A. Bridge [e], Justin R. Davis [f]

[a] *University of Maryland, College Park, Maryland, USA, mlwii@umd.edu*
[b] *University of Maryland, College Park, Maryland, USA, bphilli@umd.edu*
[c] *University of Maryland, College Park, Maryland, USA, plferndz@umd.edu*
[d] *University of Florida, Gainesville, Florida, USA, masters@eng.ufl.edu*
[e] *University of Florida, Gainesville, Florida, USA, jennifer.bridge@essie.ufl.edu*
[f] *University of Florida, Gainesville, Florida, USA, justin.r.davis@essie.ufl.edu*
[*] *Corresponding author: 4298 Campus Dr., College Park, MD 20742*

ABSTRACT: This paper explores the use of a cyber-physical systems (CPS) approach to optimize the design of rigid, low-rise structures subjected to wind loading, with the intent of producing a foundational method to study more complex structures through future research. The CPS approach combines the accuracy of physical wind tunnel testing with the ability to efficiently explore a solution space using numerical optimization algorithms. The approach is fully automated, with experiments executed in a boundary layer wind tunnel (BLWT), sensor feedback monitored by a computer, and actuators used to bring about physical changes to a mechatronic structural model. Because the model is undergoing physical change as it approaches the optimal solution, this approach is given the name "loop-in-the-model" optimization.

Proof-of-concept was demonstrated for a low-rise structure with a parapet wall of variable height. Parapet walls alter the location of the roof corner vortices, reducing suction loads on the windward facing roof corners and edges and setting up an interesting optimal design problem. In the BLWT, the parapet height was adjusted using servo-motors to achieve a particular design. Experiments were conducted at the University of Florida Experimental Facility (UFEF) of the National Science Foundation's (NSF) Natural Hazard Engineering Research Infrastructure (NHERI) program.

KEYWORDS: cyber-physical systems; mechatronic; optimization; boundary-layer wind tunnel; parapet; UFEF; NHERI

1 INTRODUCTION

Boundary layer wind tunnels (BLWT) are the primary tool in wind engineering to characterize surface pressures on bluff bodies. BLWT modeling is valuable when studying new structures for which the simplified provisions of ASCE 7 are inadequate or too conservative [1]. While BLWT modeling has remained a standard for decades, it has not benefited from recent advances in computationally-based optimization techniques for structural design. These techniques are now efficient enough to be applied during live testing if the structure has the ability to morph, e.g., change aerodynamic shape. Meta-heuristic algorithms such as particle swarm and genetic algorithms are problem-independent algorithms that efficiently explore a complex solution space, providing new opportunities to study multi-variate and multi-objective optimization problems. These optimization algorithms have promise for delivering cost-effective design solutions for wind-sensitive structures. Moreover, the accuracy of the numerical optimization process can be improved by combining it with an experimental method such as BLWT modeling.

The goal of the study is to explore the use of cyber-physical systems (CPS) for optimal design in wind engineering. We demonstrate proof-of-concept for cyberinfrastructure-augmented BLWT modeling that produces optimal designs faster than purely experimental methods and with a higher degree of realism than purely computational methods. The approach is fully automated, with experiments executed in a BLWT, sensor feedback monitored and analyzed by a coordinating computer, and optimization techniques used to bring about physical changes to the structural model in the BLWT (see Figure 1). Because the model is undergoing physical change as it approaches the optimal solution, this approach is given the name "loop-in-the-model" testing.

The building selected for the proof-of-concept was a low-rise structure with a parapet wall of variable height. The windward roof edges on low-rise structures cause a separation of the boundary layer and generate vortex flow with large suction loading that is particularly severe for oblique approaching wind angles. Changing the parapet height has a significant effect on these wind suction loads because it alters the location of the roof corner vortex, which mitigates extreme corner and edge suction loads with the tradeoff of increasing the downward roof loads in certain cases [2-5]. In this study, the model parapet height was adjusted automatically using servo-motors to create a particular design that is a "candidate" in the optimization framework. The building envelope was instrumented with pressure taps to measure the envelope pressure loading. The taps were densely spaced on the roof to provide sufficient resolution to capture the change in roof corner vortex formation. A modified particle swarm optimization (PSO) algorithm was implemented to achieve optimum parapet height which minimized suction on the roof and parapet surfaces. Experiments were conducted in the BLWT located at the University of Florida Experimental Facility (UFEF) of the National Science Foundation's (NSF) Natural Hazard Engineering Research Infrastructure (NHERI) program.

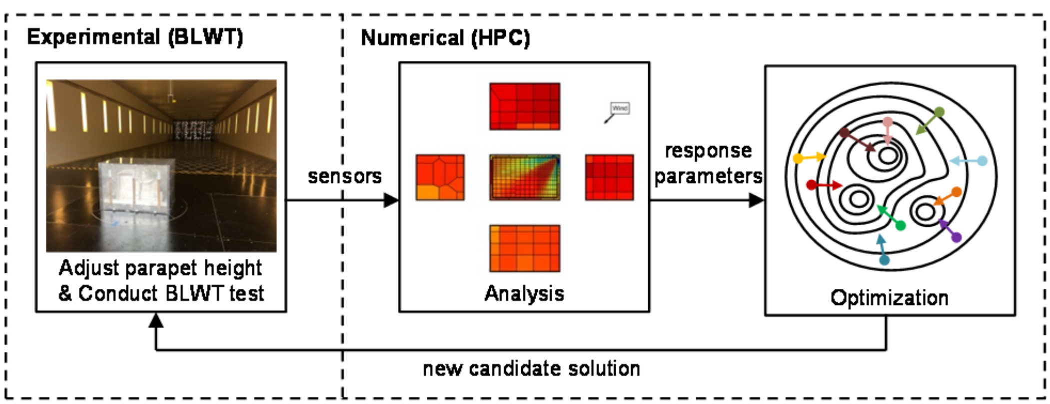

Figure 1. Diagram of CPS framework for optimal design under wind loading

2 CPS OPTIMIZATION FRAMEWORK

CPSs link the real world with the cyber world, leveraging the capabilities of computers to monitor and control physical attributes [6]. Common components of CPSs include sensing, actuation, and communication systems for interfacing, computation for executing numerical models or algorithms, and a physical phenomenon of interest. The applications for CPS in civil engineering are diverse, including hybrid simulation [7-9], online health monitoring and model updating [10], and decision-making frameworks [11]. In civil engineering, experimental testing is essential to capture complex behavior for which numerical models are insufficient, e.g., strong nonlinearities, new devices and materials, and complex loads such as wind loads on bluff bodies. Physical models that capture these behaviors can be linked to numerical algorithms to create a versatile cyber-physical framework. Experimental testing has experienced a revolution through the use of CPS. Applications including the substructuring of physical systems and the substructuring of optimization algorithms are explored below.

In civil engineering, the first use of CPS as an experimental method began in earthquake engineering with what is now known as hybrid simulation [7,12,13]. Hybrid simulation is a type of hardware-in-the-loop (HIL) test where the structural system is separated into numerical and experimental components that are linked together through a loop of action and reaction using actuators and sensors. In this way, the entire structural system is evaluated with a cost savings in the numerical components and enhanced realism in the experimental components. Hybrid simulation traditionally uses an extended time-scale for the experimental components, capturing the quasi-static nonlinear behavior of the specimen while modeling damping and inertia numerically. The development of rate-dependent structural control devices such as base isolation bearings and fluid dampers spurred interest in expanding hybrid simulation to run both experimental and numerical components in real time. The first modern real-time hybrid simulation (RTHS) was conducted by Nakashima et al. on a SDOF system [14].

Figure 2 shows an incomplete set of applications of CPS in civil engineering with a focus on experimental testing in earthquake and wind engineering. HIL testing has been developed for earthquake engineering in the form of hybrid simulation and RTHS. Similar HIL frameworks can be developed for wind engineering to study complex problems such as progressive failure and fluid-structure interaction, represented by the dashed boxes with X's under the *Hardware-in-the-Loop Testing* group in Figure 2.

Another opportunity for CPS in civil engineering is a substructuring of the optimization process, shown in the *Cyber-Physical Optimization Group* in Figure 2. Key to this framework is the numerical exploration of the design space coupled with the experimental creation and evaluation of a candidate designs. Experimental evaluation can take the form of either traditional testing methods (e.g., BLWT) or HIL methods (e.g., RTHS). The former is explored in this paper using a mechatronic specimen to explore candidate designs subject to accurate wind loading created using a BLWT. This application is termed "loop-in-the-model" optimization (LIMO) because the model is iteratively adapting toward an optimal configuration. The name is complementary to "model-in-the-loop" or "hardware-in-the-loop" testing where instead of substructuring a physical system, a physical system's properties are iteratively adjusted through optimization. Additional possibilities for cyber-physical optimization are identified with dashed boxes and X's in Figure 2, for example, hardware-in-the-loop optimization (HILO), which combines HIL testing with LIMO.

There are many opportunities for developing new cyber-physical experimental techniques across civil engineering as identified in Figure 2. This study takes a new approach, namely the substructuring of the optimization process, to create a new family of experimental methods with rich possibilities for improving structural design.

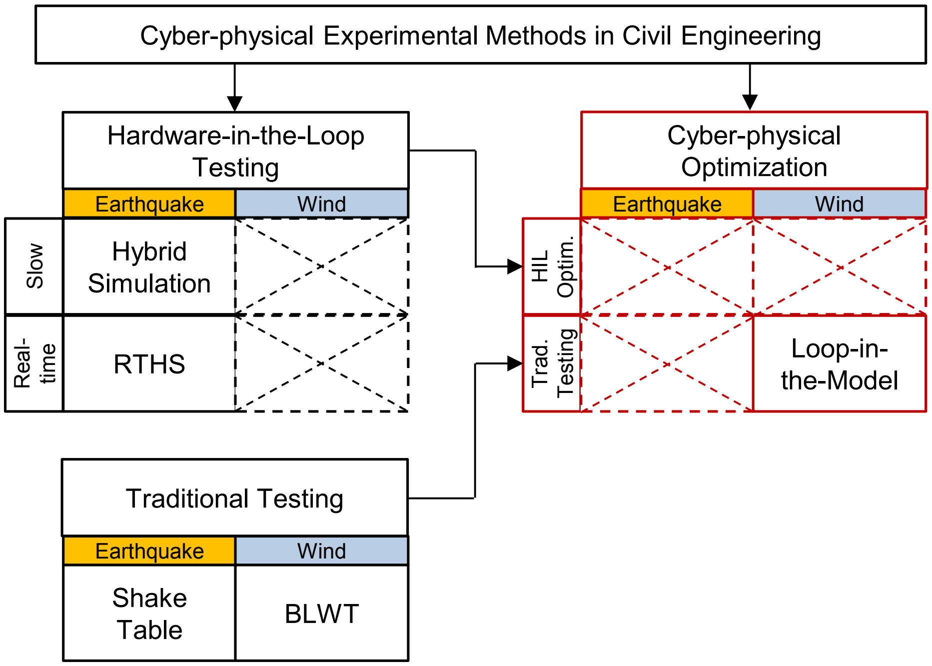

Figure 2. CPS experimental methods in earthquake and wind engineering.

3 OPTIMIZATION ALGORITHMS

A cyber-physical optimization framework (e.g. LIMO) can be built around any optimization algorithm by replacing the evaluation of a numerical model with physical testing. Popular optimization algorithms are broadly categorized as gradient-based or metaheuristic. Metaheuristic algorithms are problem independent and better suited for solving multi-objective and constrained problems without the need for gradient information [15-16]. These algorithms broadly explore candidate solutions within a search space to avoid premature or local convergence, which can lead to non-intuitive solutions for complex optimization problems. At the same time, metaheuristics are stochastic in nature, and therefore there is no guarantee that a global optimal solution, or even bounded solution, will be found [17].

Particle swarm optimization (PSO) is the metaheuristic algorithm selected for the proof-of-concept in this study. PSO mimics social behavior where a population of individuals (swarm) adapts to its environment by discovering and jointly exploring promising regions. This swarm intelligence method is based on the simulation of social interactions of members of a species, such as the movement of flocks of birds, schools of fish, and swarm of bees. Its development was inspired by evolutionary programming, genetic algorithms, and evolution strategies and shares similarities with genetic algorithms and evolutionary algorithms.

In the context of structural engineering, the swarm represents a group of candidate design solutions. Each particle within the swarm is a candidate design which consists of an N-dimensional finite position and velocity. The position refers to the values of N design parameters (e.g., parapet height of the structure) while the velocity refers to the change in the design parameters from one iteration to the next. The position of the particles is often initially randomly distributed throughout the design space. The swarm of particles then iteratively moves throughout the search space seeking better positions with the goal of discovering the global best solution. At each iteration, the particles' historic best costs and the swarm's historic best cost are updated and used to determine the next particle positions. This process is repeated either for a predetermined number of design iterations, or until user-defined convergence is reached.

The process for updating the position of each particle is

$$x_{j+1}^{i} = x_{j}^{i} + v_{j+1}^{i}\Delta t \tag{2.1}$$

where x_{j+1}^{i} is the position of particle i at iteration $j+1$, v_{j+1}^{i} is the corresponding velocity vector of the particle, and Δt is the time step value.

The procedure for determining the velocity vector of each particle in the swarm depends on the particular PSO algorithm. The equation commonly used for updating the velocity vector was first introduced by Shi and Eberhart as

$$v_{j+1}^{i} = wv_{j}^{i} + c_1 r_1 \frac{\left(p_{j}^{i} - x_{j}^{i}\right)}{\Delta t} + c_2 r_2 \frac{\left(p_{j}^{g} - x_{j}^{i}\right)}{\Delta t} \tag{2.2}$$

where r_1 and r_2 are independent random numbers in the range [0,1], p_{j}^{i} is the best known position of particle i considering iterations 1 through j, p_{j}^{g} is the best known position of all particles considering iterations 1 through j, and Δt is the time step value [18]. A unit time step of one iteration is often used for Δt. In Equation 2.2, there are three problem-dependent parameters that influence every particle's velocity: the inertia of the particle, w and two trust parameters, c_1 and c_2. The inertia controls the algorithm's exploration properties; a larger inertia enables a more global search of the design space because particles are more inclined to continue on their previous trajectory. The trust parameters indicate how much confidence the current particle has in itself, c_1 and in the swarm, c_2 and will draw the particle to these respective best positions. The selection of inertia and trust weights are problem dependent and their values must be determined case-by-case. A poor selection of parameters may lead to premature convergence to a solution that is not globally optimal, or at the other extreme, a solution that takes an excessive number of iterations to converge. Parameter selection can be made through trial and error or deduction and personal judgment.

4 PROOF-OF-CONCEPT MODEL DEVELOPMENT

Proof-of-concept for the CPS optimization framework is demonstrated for a low-rise building with a parapet wall of variable height. The parapet height was controlled using linear stepper motors. A single controllable design variable is sufficient for proof-of-concept and by limiting the study to a single design variable, unnecessary mechanical complexity was avoided and focus was instead placed on the optimization framework. While linear mechanical actuation was used herein, other mechanical and material solutions can actuate more complex models. For example, inflatable bladders or soft actuators can create controllable smooth geometries, smart materials can create discrete changes in envelope features, and stiffness and damping changes can alter the dynamic behavior of aeroelastic specimens. This CPS approach inherently loses some of the flexibility of numerical modeling by requiring physical changes; however it produces realistic loading on a structure through BLWT modeling.

In general, this CPS approach can be applied if the design parameter of interest can be controlled using a mechatronic specimen. For example, Elshaer et al. [19] explored the performance enhancement of tall buildings by optimizing the corner geometries using computational fluid dynamics (CFD). This problem can be recreated in a BLWT using a model with expandable bladders capable of creating a range of corner geometries. It is important when using this CPS approach to consider the search space for the optimization problem when designing the specimen. This approach can only consider changes which are physically possible.

4.1 *Effects of wind on low-rise buildings with parapets*

Architectural detailing has a large influence on the distribution of pressures over a roof surface in magnitude, direction, and correlation. Wind approaching at oblique angles to a building with a flat roof produces strong vortices near the upwind corner and edges of the roof [20]. These vortices are similar to the vortices that are produced at the leading edge of delta type wings and, as such, are also known as delta wing vortices. These vortices create an area of high suction on the surface of the roof near the corner [21]. Parapet walls reduce these suction loads, preventing roof gravel and other loose material from becoming wind-borne debris that can damage a building's envelope and lead to wind and rain intrusion. Solid, continuous perimetric parapets taller than 1 m act to reduce both the mean and peak pressure coefficients most notably in the corner region of these buildings [22]. Most research regarding parapets has focused on characterizing the local pressure distributions on the roof surface, specifically for components and cladding. Some studies propose the use of parapets with non-uniform or modified geometries to reduce the extreme suction loads caused by the corner vortices [2]. Additionally, a few studies consider the effect of parapets on the underlying structural members [3, 23]. Recent studies reveal that it is essential to have a high density of pressure taps in the upwind corner region to ensure that the peak suction pressures are captured [2, 3, 20].

Most building codes, such as ASCE 7-10, allow for a pressure reduction over different regions of a roof in the presence of parapets; however there has not been extensive research conducted regarding accurate regions of reduction based upon the geometry of the building and parapet or on the optimal height of a parapet for a given low-rise building [1]. Additionally, research has primarily focused on the corner zones of roofs with limited research focusing on the edge and interior zones. The research regarding the edge and interior zones has mainly focused on mitigating local loading through the use of alternative geometries and not much regarding the effect of different heights of solid, perimetric parapets or on the optimal height of solid perimetric parapets [5].

4.2 *Model actuation*

The design parameter selected is the parapet wall height of a low-rise building. Candidate design solutions must be physically created in the BLWT such that their envelope wind loads are accurately measured. The outer wall of the model was actuated by four stepper motors, one at each corner of the model. The inner core of the model remained stationary, maintaining a constant building height. As the outer wall rose above the inner model, a parapet wall was created. Strips made from polytetrafluoroethylene (PTFE) were used between the inner model and outer wall to assist in achieving smooth linear actuation. A foam gasket was used between the outer wall and the turntable to allow the outer wall to move while preventing air from leaking around the model. The model is shown in Figure 3, including the inner model (stationary) and outer wall (vertically movable).

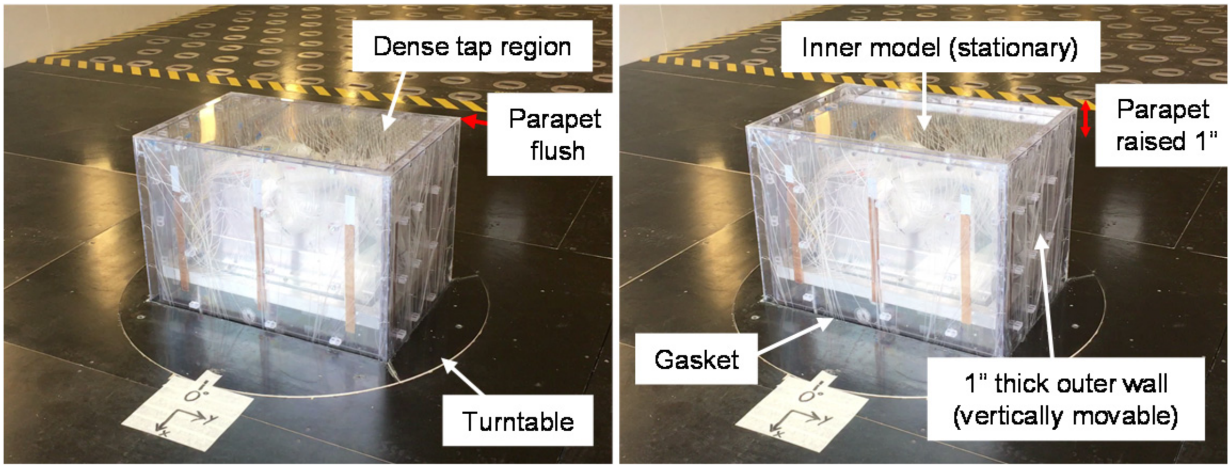

(a) (b)

Figure 3. (a) Building model with a 0 inch parapet wall and (b) a 1 inch parapet wall

Nanotec stepper motors with a captured lead screw raised and lowered the outer wall around the inner core of the model to change the eave height. The motors connected to the outer wall using polycarbonate triangular supports installed in the bottom corners. A PVC pipe installed around the drive shaft of the stepper motor protected the shaft from coming into contact with any urethane pressure tap tubing during actuation. The stepper motor and its installation are shown in Figure 4. The setup for controlling the stepper motors is given in Figure 5. Data (i.e., commands from the coordinating computer on the UF network) and power passed through a slip ring on the BLWT turntable. A Raspberry Pi 3 was mounted within the turntable to take commands from the coordinating computer and send to each of the four stepper motor controllers, which in turn actuated the stepper motors. Encoders on the stepper motors provided feedback to ensure the desired displacement was reached.

(a) (b)

Figure 4. (a) Stepper motor and (b) stepper motor installed in corner of parapet wall with PVC shield

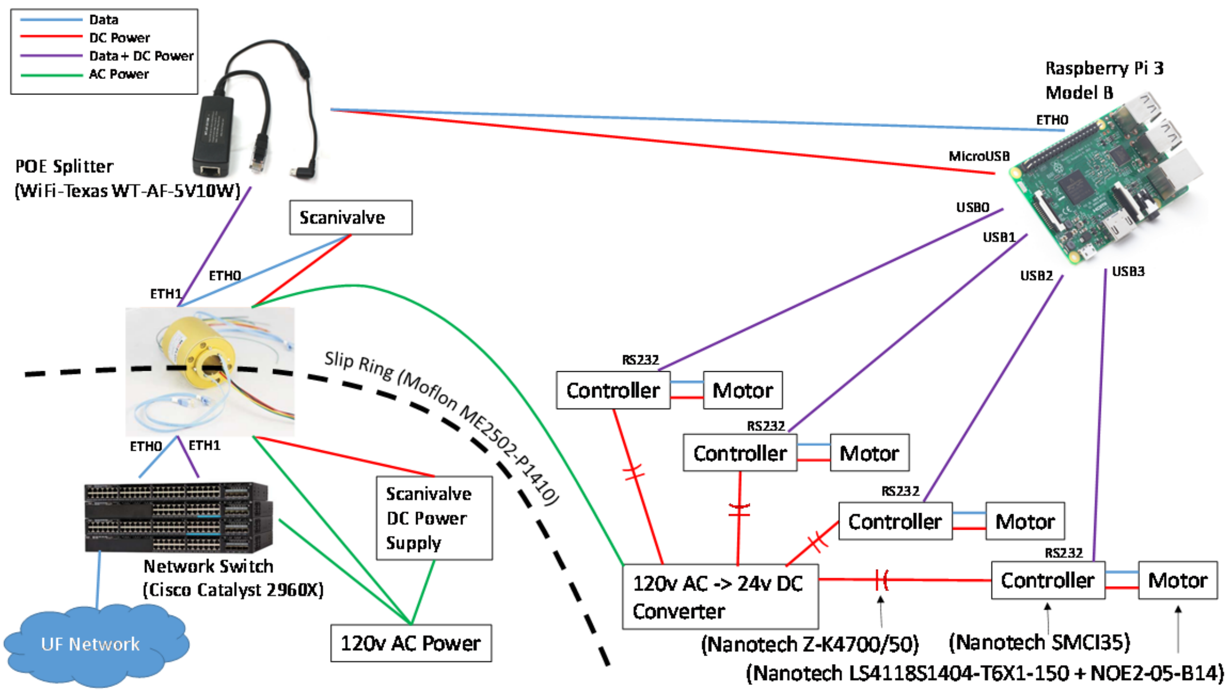

Figure 5. Wiring diagram for stepper motor control

4.3 *Model Geometry*

The low-rise building was modeled after a two-story office building. A length-to-width ratio of 1.5 was selected to create a rectangular building shape. Model dimensions were selected as 29.25 inches × 19.50 inches in plan with a height of 20 inches. By actuating the outer wall, a parapet wall of up to 4.5 inches model-scale was created. Urethane tubing and pressure taps were installed on the outer and inner sides of the parapet wall. A total thickness of the model parapet wall (and thus outer wall) of at least 1 inch was required to accommodate the thickness of polycarbonate sheets, metal tubulation, and minimum bend radius for the urethane tubing. The pressure taps on the outer and inner parapet walls were staggered to permit a thinner model parapet wall.

Based on the model dimensions and target design of a two-story office building, a 1:18 model-scale was selected. This corresponds to a building with full-scale dimensions of 29.6 feet × 44.4 feet in plan, 30 feet tall, and a 1.5 foot thick parapet. According to the Building Code Requirements for Masonry Structures, parapet walls should have a thickness of at least 8 inches [24]. The building model represents a realistic two-story full-scale building with a two by three bay steel frame.

5 CYBER-PHYSICAL EXPERIMENTAL SETUP

In the proof-of-concept developed for this paper, the loop-in-the-model optimization was driven by a numerical optimization algorithm executed in MATLAB on a coordinating computer [25]. The algorithm determined which candidate designs to evaluate, after which the cyber-infrastructure actuated the specimen to physically create these designs in the BLWT. The pressures on the model building surfaces were measured using pressure scanners and metadata was recorded for the atmospheric pressure, reference wind velocity, and humidity. Tests were repeated over all desired wind angles. The data and metadata were accessed by the coordinating computer where a MATLAB script evaluated the objective function for each candidate design. The optimization algorithm used the results for each candidate design within an iteration to determine the candidate designs for the next iteration. After testing, data and metadata were stored in the data repository of the NHERI DesignSafe web portal for later access by researchers [26].

The communication framework between the cyber and physical components is shown in Figure 6, a complement to the wiring diagram of Figure 5. The coordinating computer runs the basic MATLAB scripts for the duration of the optimization. The MATLAB scripts execute python scripts to interface with external systems, including the UFEF's BLWT Control Computer to change the specimen angle, Scanivalve for data acquisition, and Raspberry Pi for motor control.

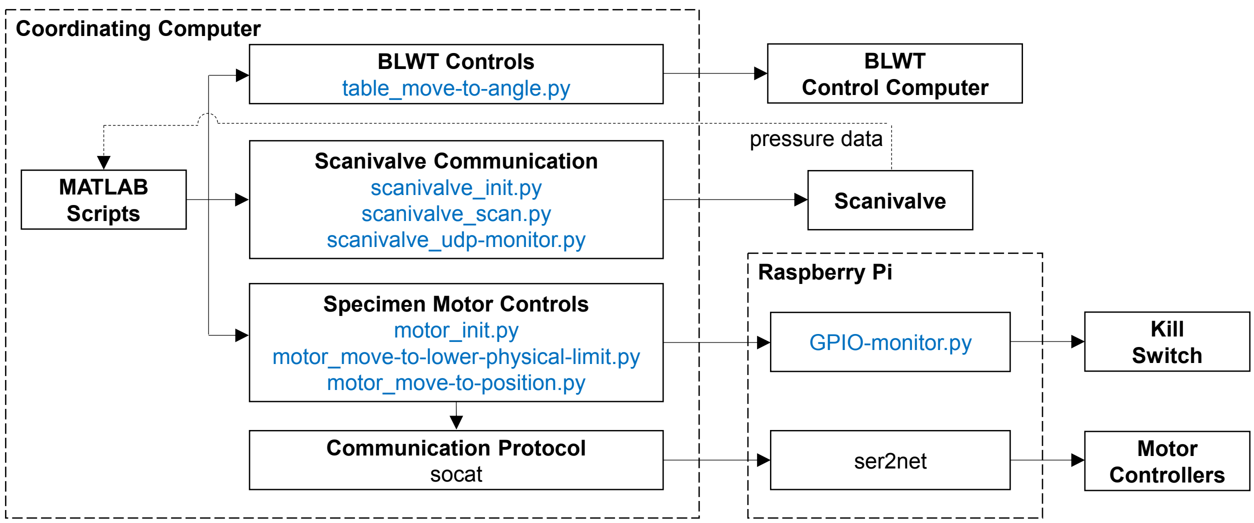

Figure 6. Links between cyber-physical components

5.1 *Experimental equipment*

Experiments were conducted in the BLWT located at the University of Florida Natural Hazard Engineering Research Infrastructure (NHERI) Experimental Facility. The BLWT is 6.1 m wide with a 1 m turntable centered along the 6.1 m width 31.75 m downwind of 8 fans. The fans were kept at 1050 RPM for all testing, which corresponds to a reference height velocity of approximately 14 m/s. The pressures on the model building surfaces were measured using Scanivalve ZOC33 [27]. The model building installed in the BLWT is shown in Figure 7.

Figure 7. Boundary layer wind tunnel with model low-rise building, upwind view

5.2 *Tap tributary areas*

The pressure measured at each pressure tap was assumed to act over a unique and non-overlapping tap tributary area on the model surface. In this model, tap locations were variable due to the moving outer wall. Based on the parapet wall height, exposed tap locations and surface areas were calculated. Then, tap tributary areas were calculated using Voronoi diagrams derived from Delaunay triangulation [28]. This process is both reproducible and automated, which was particularly important because the geometry of the building changes with every candidate solution. The taps and tributary areas for the model with a parapet wall of 5 inches are depicted in the flattened view of Figure 8. The walls of the building are given by Surfaces 1 to 4. As the walls extended above the roof (from actuation), Surfaces 1 to 4 also formed the outer parapet walls. The inner parapet walls are given by Surfaces 6 to 9. The edges that join the outer walls (Surfaces 1 to 4) and the inner parapet walls (Surfaces 6 to 9) in Figure 8 are at the same height in the model. Surfaces 5 and 10 are the top of the parapet wall and the roof, respectively. As the parapet height increased, the tributary areas for both the outer wall and inner parapet walls increased while the tributary areas for the top of the parapet wall and the roof remained constant.

Published Version at: Whiteman, M.L., Phillips, B.M., Fernández-Cabán, P.L., Masters, F.J., Bridge, J.A., and Davis, J.R. (2018). “Optimal Design of Structures using Cyber-physical Wind Tunnel Experiments with Mechatronic Models.” Journal of Wind Engineering and Industrial Aerodynamics, 172. DOI: 10.1016/j.jweia.2017.11.013.

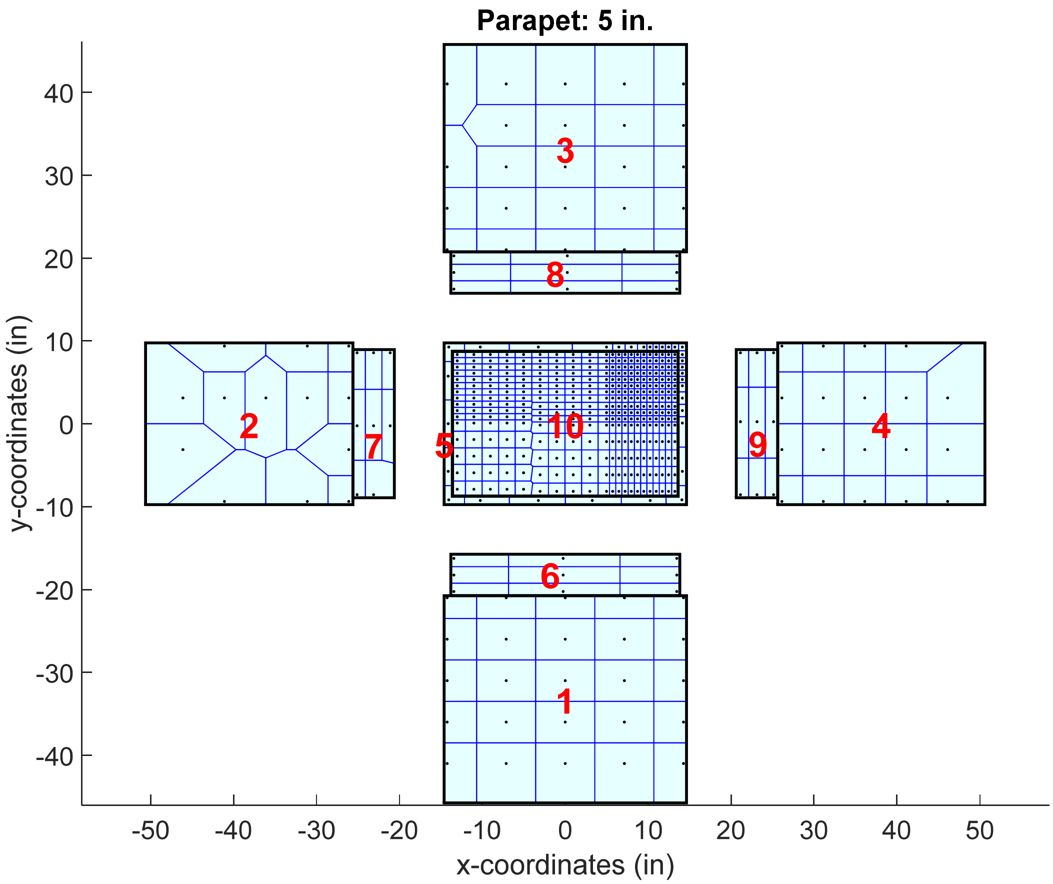

Figure 8. Tap locations and tributary areas on a flattened representation of the model with a parapet of 5 inches

5.3 *Wind simulation*

Simulation of upwind terrain roughness was performed via the Terraformer, an automated roughness element grid that rapidly reconfigures the height and orientation of 1116 roughness elements in a 62 × 18 grid to achieve desired upwind terrain conditions [29]. The grid has a fetch length of 18.3 m. Dimensions of the elements are 5 cm by 10 cm, and they are spaced 30 cm apart in a staggered pattern. Height and orientation can be varied from 0-160 mm and 0-360 degrees, respectively. For this study, the Terraformer was configured to simulate open terrain for the given geometric scale (1:18).

Prior to placing the model in the tunnel, flow measurements were taken at the center of the test section using an automated gantry system instrumented with four Turbulent Flow Instrumentation Cobra pressure probes that measure u, v, and w velocity components and static pressure. For this study, roughness elements were raised to 20 mm and oriented with the wide edge perpendicular to the flow. Figure 9 includes the mean velocity profile and the measured longitudinal turbulence spectra at a height of 610 mm. The mean velocity profile was normalized by the reference mean wind velocity U_{ref} measured at a height $z_{ref} = 1.48$ m. A roughness length estimate of 1.59 mm was obtained from a non-linear least-squares fit of the log law in the inertial-sublayer (ISL) region (z ~ 150-900 mm), following the curve-fitting method in Karimpour et al. [30]. This results in an equivalent full-scale roughness length of 0.029 m, which

Final Accepted Version
Published Version at: Whiteman, M.L., Phillips, B.M., Fernández-Cabán, P.L., Masters, F.J., Bridge, J.A., and Davis, J.R. (2018). "Optimal Design of Structures using Cyber-physical Wind Tunnel Experiments with Mechatronic Models." Journal of Wind Engineering and Industrial Aerodynamics, 172. DOI: 10.1016/j.jweia.2017.11.013.

is within the range of open terrain as defined in ASCE 7-10. The measured spectra was compared with the power spectra model in ESDU [31], and first derived by von Kármán for isotropic turbulence [32]. The measured longitudinal integral length scale (L_u^x) in the tunnel at z = 610 mm was 1.06 m. For a 1:18 simulation, this results in a full-scale L_u^x = 18 m (z ~ 11 m), which is ~16% of the expected L_u^x for open terrain – e.g., for z_0 = 0.03 m and z = 10 m, L_u^x = 110 m [33]. The challenges associated with achieving sufficient length scales of turbulence in the BLWT for large models (e.g., low-rise buildings) are well established [34, 35]. The discrepancy in L_u^x (model versus full-scale) arises from the absence of large-scale turbulence in the BLWT. Recent methods, such as partial turbulence simulation [36], have been successful in compensating for a lack of large-scale turbulence. Nevertheless, the mismatch in integral lengths does not detract from the fundamental objective of applying CPS approaches in the BLWT.

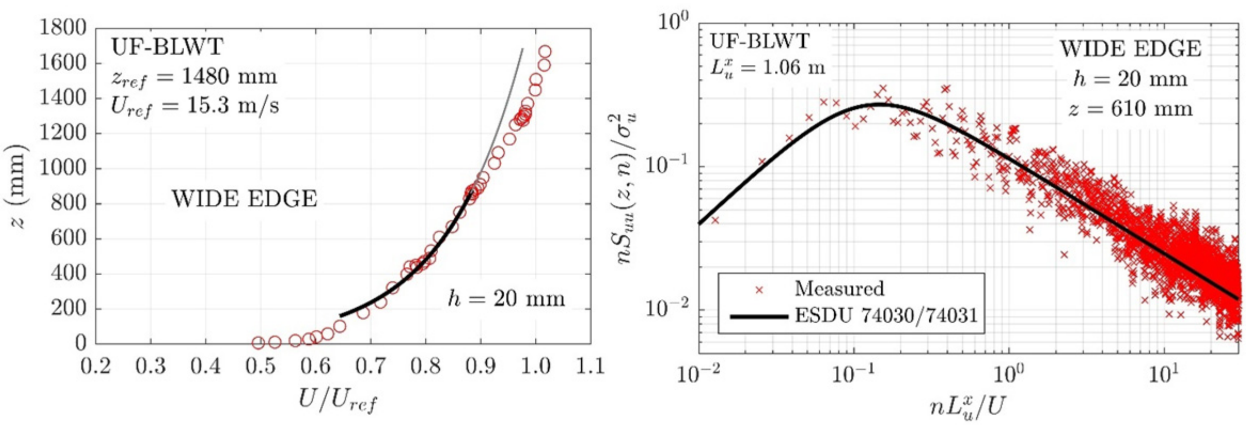

(a) (b)

Figure 9. (a) Mean velocity profile and (b) longitudinal turbulence spectra (z = 610 mm) measured at the center of the test section for h = 20 mm and a wide edge windward element orientation.

5.4 *Pressure coefficients*

Differential pressures from 512 taps were measured simultaneously and sampled at 625 Hz. Data was collected for 120 seconds, corresponding to approximately 660 seconds full-scale assuming a basic wind speed of 40 m/s at reference height. Pressure coefficients were referenced to the velocity pressure at the model eave height. This velocity pressure was obtained indirectly by applying a reduction factor to pitot tube measurements at the freestream (z = 1.48 m). Maximum and minimum pressure coefficients were estimated from each tap pressure time history using a Fisher-Tippett Type I (Gumbel) distribution [37]. The C_p time history was truncated into 50 segments of equal length. The peak maximum and minimum pressure coefficients from each segment were then taken, and the 78th percentile is then used to estimate the maximum and minimum C_p values.

6 OPTIMIZATION

The optimization problem was physically constrained by the model-scale minimum and maximum parapet height of 0 and 4.5 inches, respectively. The lower and upper physical bounds were chosen such that the optimal solution would confidently be located within the search space. Considering the time limits on experimental resources, a balance was needed between sufficient particles to create the PSO swarm effect and sufficient iterations to converge. Based on an estimated two minutes per BLWT run, one minute to set up the BLWT run, and a day of testing, five particles were selected.

The objective function was selected as a minimization of the suction on the roof, inner parapet walls, and top of the parapet considering all wind angles (Surfaces 5-10) in Figure 8. As the parapet height increased, the suction decreased for the roof surface and top of the parapet wall and increased for the inner parapet wall surfaces. Critical minimum C_p values were observed for the roof, inner parapet wall, and top of parapet at approach wind angles of 45° and 90° (Figures 10 and 11). To minimize the number of BLWT runs, each candidate solution was only evaluated at 45° and 90° with the dense roof taps upwind.

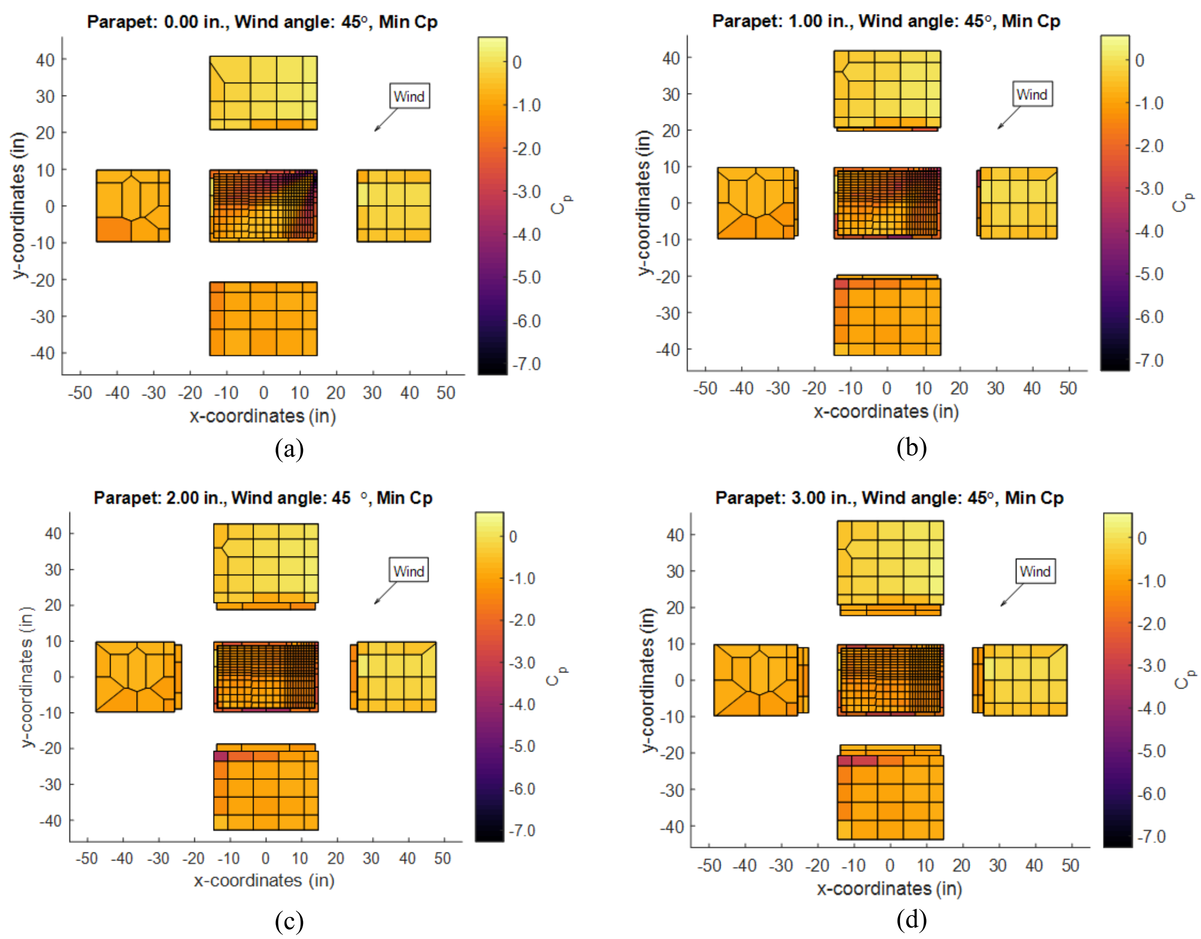

Figure 10. Minimum C_p for 45°, (a) 0 inch parapet, (b) 1 inch parapet, (c) 2 inch parapet, and (d) 3 inch parapet

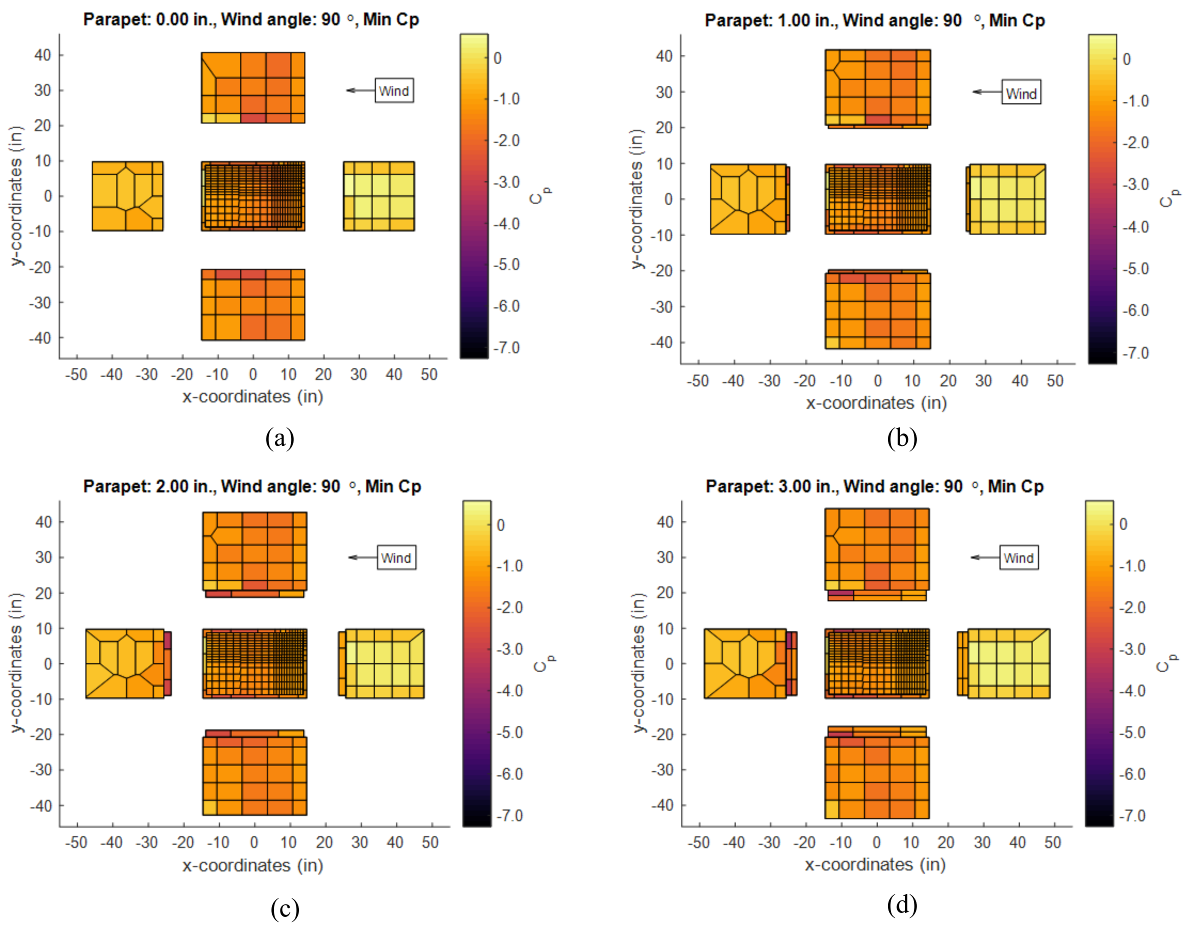

Figure 11. Minimum C_p for 90°, (a) 0 inch parapet, (b) 1 inch parapet, (c) 2 inch parapet, and (d) 3 inch parapet

The experiments were driven by a modified PSO algorithm. Modifications were made to increase the computational efficiency and reduce the number of experiments required. Traditional PSO does not address particles which violate design constraints. Thus, constrained optimization was introduced to address this problem through the use of a fly-back mechanism. In the traditional fly-back mechanism, a particle that would violate a design constraint is prevented from moving for that iteration. The algorithm proceeds as normal for the next iteration. The global minima (or maxima, depending on objective) of design problems are often close to the boundaries of the feasible search space [38]. The traditional fly-back mechanism will exploit solutions around the boundaries. In this study, the solution is not expected to be near the boundaries. Therefore, in addition to preventing the particle from moving beyond the boundary, the direction of the velocity is reversed (i.e., the velocity now points away from the boundary). This modification enables better exploration of the interior of the search space.

The cyber-physical optimization approach specialized for PSO, a predetermined set of evaluation wind angles, and the proof-of-concept parapet model is shown in Figure 12. Loops over all angles, all particles, and all iterations are highlighted to clearly illustrate the experimental timeline.

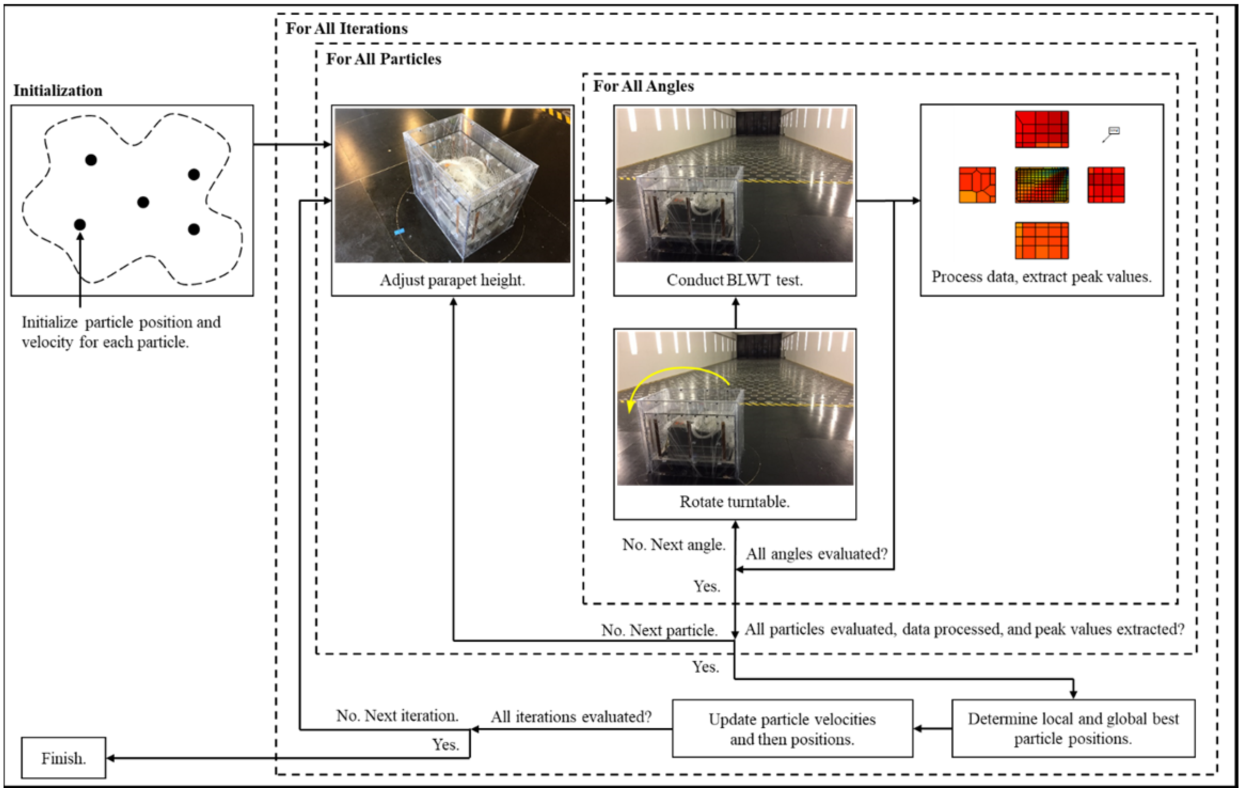

Figure 12. Cyber-physical optimization approach as implemented with PSO

7 OPTIMIZATION RESULTS AND ANALYSIS: CASE 1

The problem-specific PSO parameters of $w, c_1,$ and c_2 are all selected as 0.5. These values produced favorable convergence for a simulated (offline) optimization run using a pre-recorded test matrix of wind angles and parapet heights. To initialize the (online) optimization run, the position of the particles was uniformly distributed across the range of positions. A total of 13 design iterations were conducted for the 5 particles. The convergence of the particles towards the optimum height of 2.69 inches is shown in Figure 13a. Four of the five particles converged to the global best cost. The one particle that did not converge is likely due to the particle being attracted to both its personal best cost (achieved at iteration 1) and the global best cost. Methods to avoid particles becoming stuck will be considered in Section 8. The global best cost for each iteration is shown in Figure 13b. Points with both particle number and cost identified represent an update to the global best cost. Figures 14 and 15 depict the envelope plot of the minimum C_p for the optimal parapet height at 45° and 90° respectively. This illustrates the balance in minimum C_p on the roof and top of the parapet wall (Figure 14) and inner parapet wall surfaces (Figure 15). This balance is expected because the suction on the roof, top of the parapet, and inner parapet walls were given equal weight in the objective function.

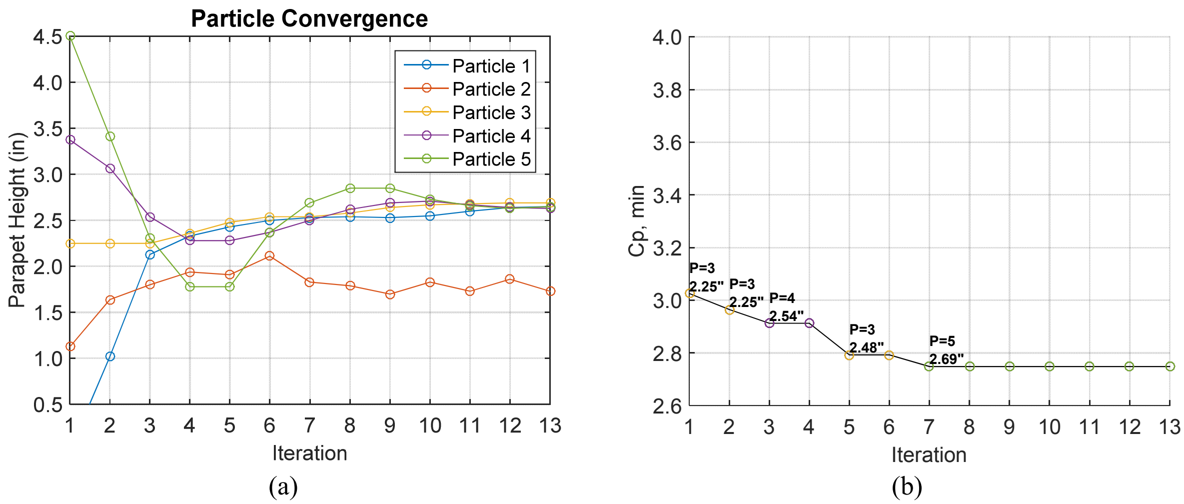

Figure 13. (a) Particle convergence at each iteration and (b) Iteration history of global best cost

The optimal result corresponds to a full-scale parapet height of 4.04 feet, an otherwise non-intuitive design. This parapet height simultaneously minimizes suction on the roof and inner parapet walls. According to the Building Code Requirements for Masonry Structures, the height of structural parapets should not exceed 3 times their thickness [24]. The optimal height found satisfies this limit of 4.5 feet as applied to the current building.

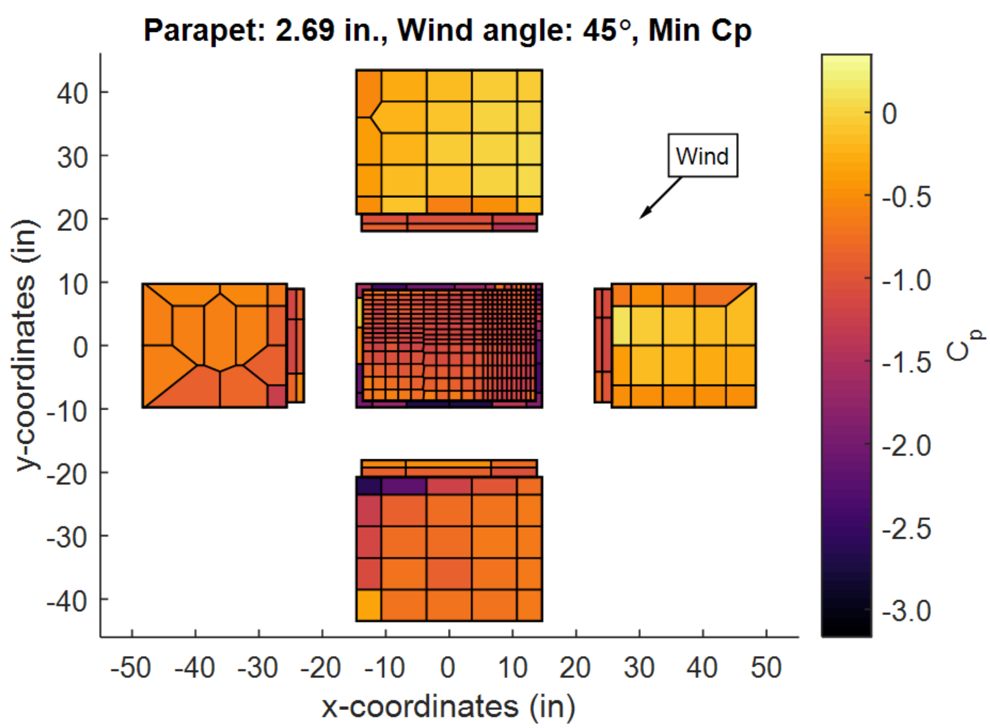

Figure 14. Minimum C_p for optimal parapet height, 45° wind angle shown

Published Version at: Whiteman, M.L., Phillips, B.M., Fernández-Cabán, P.L., Masters, F.J., Bridge, J.A., and Davis, J.R. (2018). "Optimal Design of Structures using Cyber-physical Wind Tunnel Experiments with Mechatronic Models." Journal of Wind Engineering and Industrial Aerodynamics, 172. DOI: 10.1016/j.jweia.2017.11.013.

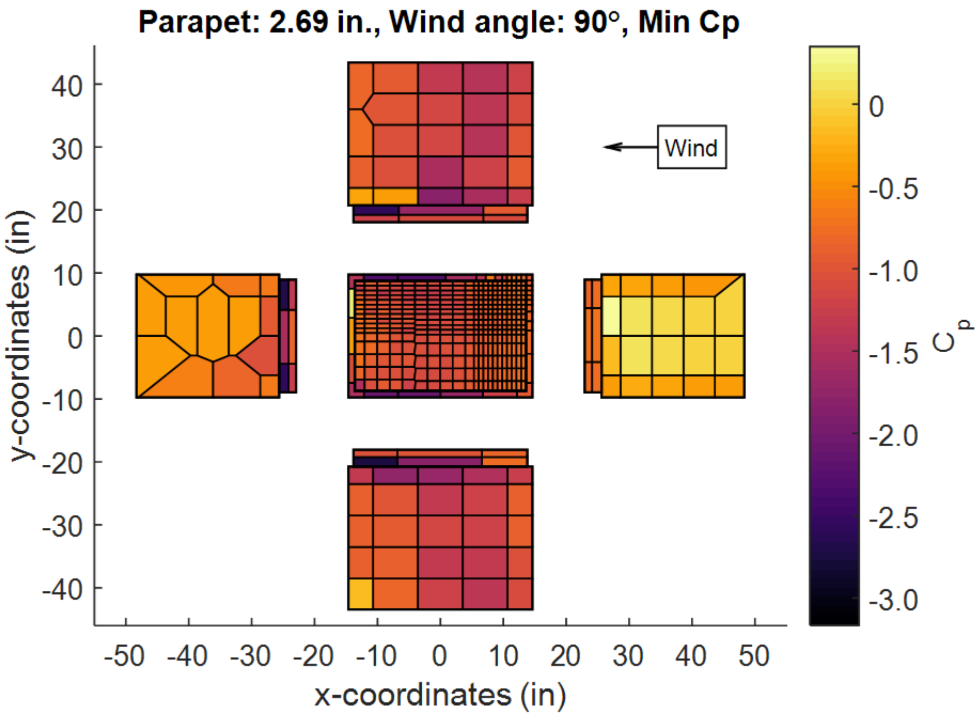

Figure 15. Minimum C_p for optimal parapet height, 90° wind angle shown

8 OPTIMIZATION RESULTS AND ANALYSIS: CASE 2

Two additional PSO modifications are proposed to improve the accuracy of the cyber-phsyical approach to optimization by addressing issues which arise with both the cyber and physical components. The issues of premature convergence (cyber) and sensitivity to outliers (physical) are identified and modifications are introduced for evaluation in a second optimization run.

8.1 *Smartest particle: avoid premature convergence*

PSO can prematurely converge to solutions found in early iterations if not properly calibrated [39]. Recalling Equation 2.2, the calculation of the velocity vector for each particle at iteration j depends on the best known position of all particles considering iterations 1 through j. If the global best position corresponds to a local optimum, then premature convergence may occur as all particles are attracted to this solution. If weight is placed on the position of the particle which found the global best position, rather than the global best position itself, then premature convergence can be avoided. This particle, the "smartest" particle, will encourage continued exploration by avoiding stagnation of the p_j^g term.

Following the current position of the global best particle rather than its global best positions leads to a new definition for velocity updates

$$v_{j+1}^i = wv_j^i + c_1 r_1 \frac{(p_j^i - x_j^i)}{\Delta t} + c_2 r_2 \frac{(x_j^g - x_j^i)}{\Delta t} \tag{8.1}$$

where r_1 and r_2 are independent random numbers in the range [0,1], w is the inertia of the particle, c_1 and c_2 are two trust parameters indicating a particle's trust in itself and trust in the swarm respectively, p_j^i is the best known position of particle i considering iterations 1 through j, x_j^g is the position at iteration j of the particle g which determined the best known position of all particles considering iterations 1 through j, and Δt is the time step value.

8.2 *Forgetting function: avoid sensitivity to outliers*

BLWT testing is subject to experimental error; results will vary from experiment to experiment, even for the same specimen configuration. Data may be associated with a specimen configuration that is not truly representative of that configuration. With regard to PSO, outlier data can affect both a particle's local best solution and the swarm's global best solution. Even if the results are not repeatable, they may be retained as the local or global best solution for the remainder of the optimization. Outliers can potentially cause convergence to a position that does not accurately represent the global best position. To address the variability of wind tunnel testing, a modification to the PSO algorithm is proposed.

A "forgetting function" is introduced to the swarm so that particles within the swarm suffer a partial loss of memory and "forget" both global and local best solutions. In evaluating global and local best costs, the modified PSO algorithm will only consider solutions that have been created within a specified number of previous iterations. The corresponding positions for this limited horizon will become the new global and local best particle positions. If the solution of a particular parapet height was the result of an outlier experiment, then it will eventually be forgotten, and the global and local best particle positions would be updated in its absence. With the forgetting function, the convergence to the global solution may no longer be monotonic.

After offline simulations using Case 1 test data, the number of iterations to consider for global and local best calculations is selected to be 5 (i.e., the current iteration and 4 previous iterations).

8.3 *Optimization results and analysis*

The problem-specific parameters of $w, c_1,$ and c_2 are selected to be 0.5, 1.0, and 1.0 respectively so that an equal weight would be placed on the particle's inertia, trust in itself, and trust in the swarm by giving the products of $c_1 r_1$ and $c_2 r_2$ each a mean of 0.5. The position of the particles was initially randomly distributed across the range of positions. A total of 15 design iterations were conducted for the 5 particles. The convergence of the particles towards the optimum height of 2.70 inches is shown in Figure 16a. The global best cost for each iteration is shown in Figure 16b, and the results are similar to those of Figure 13b. Figures 17 and 18 depict the envelope plot of the minimum C_p for the optimal parapet height at 45° and 90° respectively, and the results are similar to those of Figures 14 and 15. The optimal result corresponds to a full-scale parapet height of 4.05 feet, an otherwise non-intuitive design which satisfies the limit of 4.5 feet according to the Building Code Requirements for Masonry Structures as applied to the current building [24].

In comparison to the modified PSO used in Case 1 which had four of five particles converge to the global best cost (Figure 13a), all five particles converged to the global best cost with the incorporation of the smartest particle (Figure 15a). The loss of diversity of individuals within a population is a symptom of premature convergence because of the loss of the exploration capabilities of the individuals. This loss of diversity can be seen in Figure 13a as multiple particles are close to one another in position and follow similar search paths, whereas the particles in Figure 16a retain their diversity.

In comparison to the modified PSO used in Case 1 which had a monotonically converging global best cost, the global best cost non-monotonically converges with the incorporation of the forgetting function. The global best position determined at iteration 10 of 2.68 inches attracts all particles to this height. Despite repeated testing of this particular position after it is found to be the global best position, the position of 2.70 inches is found to produce a better cost once the particular test at iteration 10 is forgotten. This suggests that the solution found to be the global best at iteration 10 was not representative of the height of 2.68 inches and can be considered an outlier. Similarly, the solution at 2.70 inches may be an outlier, which would be revealed by continued testing.

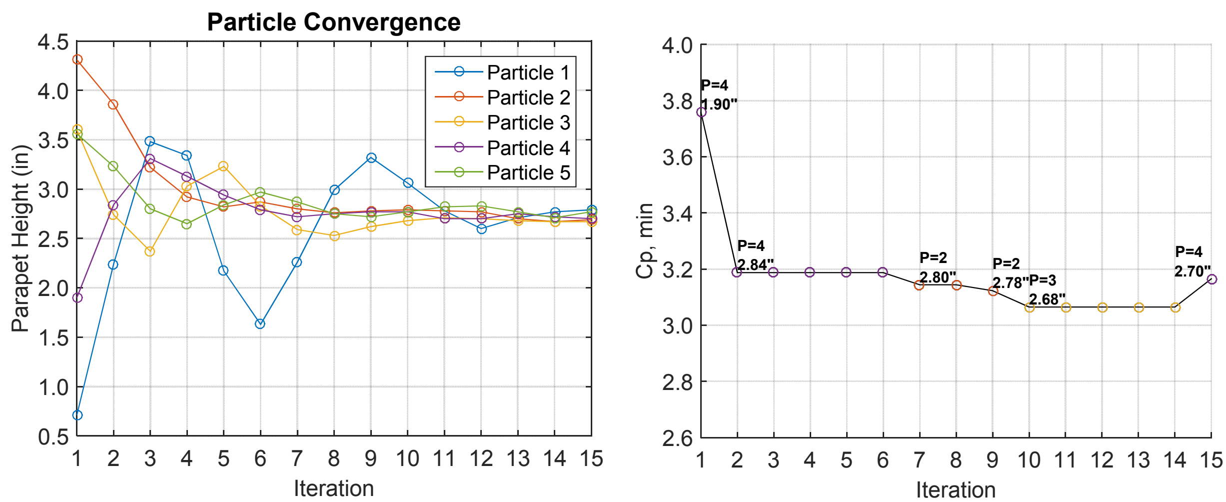

(a) (b)

Figure 16. (a) Particle convergence at each iteration and (b) Iteration history of global best cost

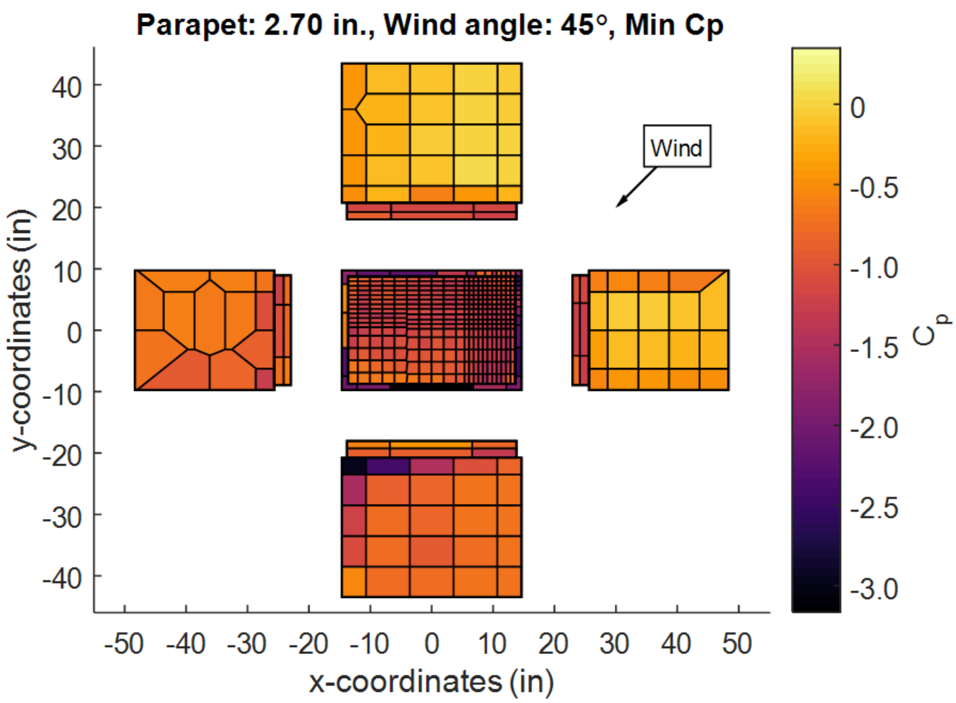

Figure 17. Minimum C_p for optimal parapet height, 45° wind angle shown

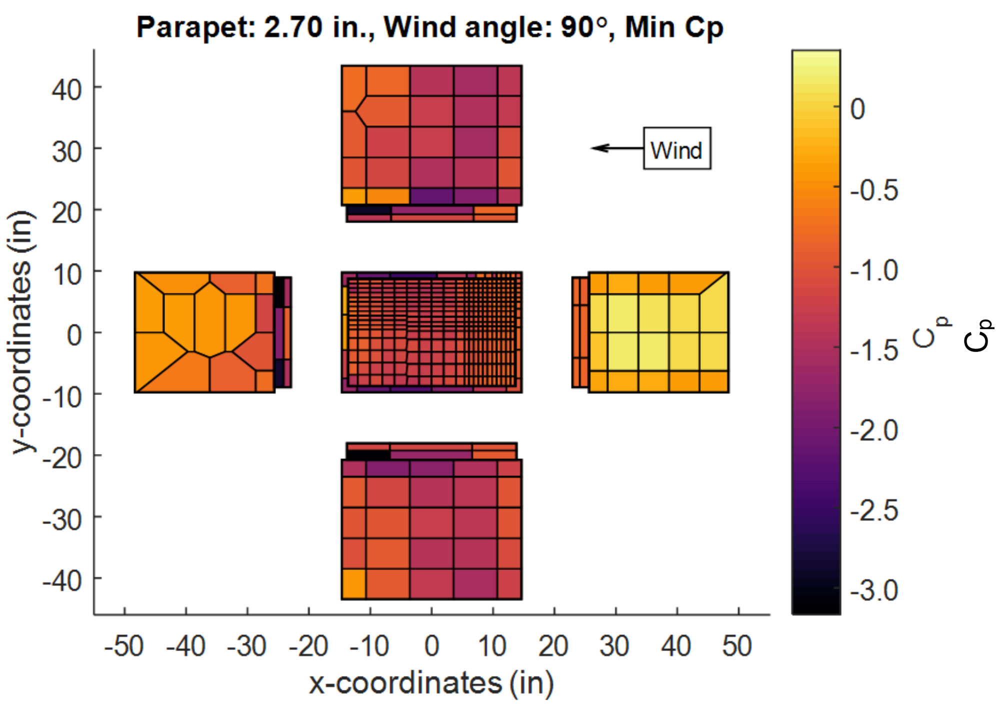

Figure 18. Minimum C_p for optimal parapet height, 90° wind angle shown

9 CONCLUSIONS

This study explores a cyber-physical system (CPS) approach to the optimal design of structures subject to wind loading. The optimization process is substructured into cyber and physical components, creating a new loop-in-the-model optimization (LIMO) framework. The analysis of data, calculation of objective functions, and determination of new candidate designs is done numerically. The creation and evaluation of candidate designs is completed physically in a boundary layer wind tunnel (BLWT) using a mechatronic specimen. The framework was demonstrated to automatically guide the physical structure to an optimal state based on user-defined objectives and constraints. The LIMO framework enables the optimal solution to be found quicker than brute force methods, in particular for complex structures with many design variables. The integration of metaheuristic search algorithms will enable the discovery of new and non-intuitive designs, all while placing the burden of design iteration on an accurate and automated system. Successful implementation will simplify and enhance the design workflow and ultimately advance our capability to build stronger and more resilient structures.

As proof-of-concept, this study investigated the effect of wind loads on low-rise buildings with a solid parapet of variable height, creating an optimization problem with a single design variable that has a non-monotonic influence on the envelope wind load. This study focuses on envelope load effects, seeking the parapet height that minimizes roof and parapet wall suction loading. The optimization algorithm selected was particle swarm optimization (PSO); however the framework is flexible and could be guided by any gradient-based (i.e., using finite differences) or metaheuristic algorithms. Based on the objective function and constraints chosen, optimal parapet heights of 2.69 inches model-scale and 4.04 feet full-scale (Case 1) and 2.70 inches model-scale and 4.05 feet full-scale (Case 2) were found for the low-rise structure studied using the modified PSO algorithms. The findings are potentially significant for more complex structures where the optimal solution may not be obvious and cannot be easily determined with traditional experimental or computational methods.

10 ACKNOWLEDGEMENTS

This material is based upon work supported by the National Science Foundation (NSF) under Grant No. 1636039. Any opinions, findings, and conclusions or recommendations expressed in this material are those of the authors and do not necessarily reflect the views of NSF. The authors also acknowledge the NSF NHERI awardee that contributed to the research results reported within this paper under Grant No. 1520843: Natural Hazards Engineering Research Infrastructure: Experimental Facility with Boundary Layer Wind Tunnel, Wind Load and Dynamic Flow Simulators, and Pressure Loading Actuators (University of Florida) and Grant No. 1520817: Natural Hazards Engineering Research Infrastructure: Cyberinfrastructure (DesignSafe).

11 REFERENCES

1 ASCE/SEI 7-10, 2010. *Minimum Design Loads for Buildings and Other Structures*. American Society of Civil Engineers, Reston, VA, USA.

2 Kopp, G. A., Surry, D., and Mans, C. "Wind effects of parapets on low buildings: Part 1. Basic aerodynamics and local loads." *Journal of Wind Engineering and Industrial Aerodynamics*, vol. 93, no. 11, 10 Oct. 2005, pp. 817–841.

3 Kopp, G. A., Surry, D., and Mans, C. "Wind effects of parapets on low buildings: Part 2. Structural loads." *Journal of Wind Engineering and Industrial Aerodynamics*, vol. 93, no. 11, 10 Oct. 2005, pp. 843–855.

4 Kopp, G. A., Surry, D., and Mans, C. "Wind effects of parapets on low buildings: Part 3. Parapet loads." *Journal of Wind Engineering and Industrial Aerodynamics*, vol. 93, no. 11, 10 Oct. 2005, pp. 857–872.

5 Kopp, G. A., Surry, D., and Mans, C. "Wind effects of parapets on low buildings: Part 4. Mitigation of corner loads with alternative geometries." *Journal of Wind Engineering and Industrial Aerodynamics*, vol. 93, no. 11, 10 Oct. 2005, pp. 873–888.

6 Al-Hammouri, A. T. "A comprehensive co-simulation platform for cyber-physical systems." *Computer Communications*, vol. 36, no. 1, 2012, pp. 8-19.

7 Shing, P. B. and Mahin, S. A. "Pseudodynamic test method for seismic performance evaluation: Theory and implementation." *UCB/EERC-84/01*, Earthquake Engineering Research Center, University of California, Berkeley, CA. 1984.

8 Takanashi K. and Nakashima, M. "Japanese Activities On-Line Testing." *ASCE Journal of Engineering Mechanics*, vol. 113, no. 7, 1987, pp. 1014-1032.

9 Shing P. B., Nakashima, M., and Bursi, O. "Application of Pseudodynamic Test Method to Structural Research." *Earthquake Spectra*, vol. 12, no. 1, 1996, pp. 29-56.

10 Song, W. and Dyke, S. "Development of a cyber-physical experimental platform for real-time dynamic model updating." *Mechanical Systems and Signal Processing*, vol. 37, no. 1, 2013, pp. 388-402.

11 Lin, S. L., Li, J., Elnashai, A. S., and Spencer Jr, B.F. "NEES integrated seismic risk assessment framework (NISRAF)." *Soil Dynamics and Earthquake Engineering*, vol. 42, 2012, pp. 219-228.

12 Hakuno, M., Shidawara, M., and Hara, T. (1969). "Dynamic destructive test of a cantilever beam controlled by an analog computer." Transactions of the Japan Society of Civil Engineers, 171:1-9 (In Japanese).

13 Takahashi, K. and Nakamura, M. (1987). "Japanese activities on on-line testing." *Journal of Engineering Mechanics*. 113(7): 1014-1032.

14 Nakashima, M., Kato, H., and Takaoka, E. (1992). "Development of real-time pseudo dynamic testing." Earthquake Engineering and Structural Dynamics, 21(1): 79-92.

15 Luke, S. (2013). "Essentials of Meta-heuristics." Lulu, 2nd Edition.

16 Talbi, El-Ghazali. *Metaheuristics: From Design to Implementation*. Hoboken (NJ): John Wiley & Sons, 2009. Print.

17 Perez, R. E., and Behdinan, K. Particle Swarm Optimization in Structural Design. *Swarm Intelligence: Focus on Ant and Particle Swarm Optimization*, 2007, pp. 373-377.

18 Shi, Y., and Eberhart, R. "A Modified Particle Swarm Optimizer." *1998 IEEE International Conference on Evolutionary Computation Proceedings. IEEE World Congress on Computational Intelligence (Cat. No.98TH8360),* pp. 69–73.

19 Elshaer, A., Bitsuamlak, G., & El Damatty, A. (2017). Enhancing wind performance of tall buildings using corner aerodynamic optimization. *Engineering Structures*, vol. 136, pp. 133-148.

20 Kind, R. J. "Worst suctions near edges of flat rooftops with parapets." *Journal of Wind Engineering and Industrial Aerodynamics*, vol. 31, no. 2-3, 1988, pp. 251–264.

21 Pindado, S., and Meseguer, J. "Wind tunnel study on the influence of different parapets on the roof pressure distribution of low-rise buildings." *Journal of Wind Engineering and Industrial Aerodynamics*, vol. 91, no. 9, 2003, pp. 1133–1139.

22 Stathopoulos, T. and Baskaran, A. "Wind Pressures on Flat Roofs With Parapets." *Journal of Structural Engineering*, vol. 113, no. 11, 1987, pp. 2166-2180.

23 Stathopoulos, T., Saathoff, P., and Du, X. "Wind loads on parapets." *Journal of Wind Engineering and Industrial Aerodynamics*, vol. 90, no. 4-5, 2002, pp. 503–514.

24 ACI/ASCE/TMS, *Building code requirements and specification for masonry structures: containing Building code requirements for masonry structures (TMS 402-11/ACI 530-11 / ASCE 5-11), Specification for mason structures (TMS 602-11 / ACI 530.1-11 / ASCE 6-11) and companion commentaries / developed by the Masonry Standards Joint Committee (MSJC)*. Boulder, Co., The Masonry Society, 2011.

25 MATLAB version 8.4.0. Natick, Massachusetts: The MathWorks Inc., 2014.

26 Rathje, E., Dawson, C. Padgett, J. E., Pinelli, J.-P., Stanzione, D., Adair, A., Arduino, P., Brandenberg, S.J., Cockerill, T., Dey, C., Esteva, M., Haan, Jr., F. L., Hanlon, M., Kareem, A., Lowes, L., Mock, S., and Mosqueda, G. 2017. "DesignSafe: A New Cyberinfrastructure for Natural Hazards Engineering," ASCE Natural Hazards Review, doi:10.1061/(ASCE)NH.1527-6996.0000246.

27 ZOC33 miniature pressure scanner. (2016). Retrieved from http://scanivalve.com/products/pressure-measurement/miniature-analog-pressure-scanners/zoc33-miniature-pressure-scanner/

28 Gierson, M. L., Phillips, B. M., Duthinh, D., and Ayyub, B. "Wind-Pressure Coefficients on Low-Rise Building Enclosures Using Modern Wind-Tunnel Data and Voronoi Diagrams." *ASCE-ASME Journal of Risk and Uncertainty in Engineering Systems, Part A: Civil Engineering*, vol. 3, no. 4, 2017.

29 Fernández-Cabán, P. L., & Masters, F. J. "Near surface wind longitudinal velocity positively skews with increasing aerodynamic roughness length." *Journal of Wind Engineering and Industrial Aerodynamics*, *169*, 2017, pp. 94-105.

30 Karimpour, A., Kaye, N. B., and Baratian-Ghorghi, Z. "Modeling the neutrally stable atmospheric boundary layer for laboratory scale studies of the built environment." *Building and Environment*, 49, 2012, pp. 203-211

31 ESDU. Characteristics of atmospheric turbulence near the ground. Part I: definitions and general information, *Engineering Sciences Data Unit*, Itm. No. 74030, 74031, 1974, London, UK.

32 Von Karman, T. "Progress in the statistical theory of turbulence." *Proceedings of the National Academy of Sciences*, vol. 34, no. 11, 1948, pp. 530-539.

33 ASCE/SEI 49-12, 2012. *Wind Tunnel Testing for Buildings and Other Structures*. American Society of Civil Engineers, Reston, VA, USA.

34 Stathopoulos, T., & Surry, D. (1983). Scale effects in wind tunnel testing of low buildings. *Journal of Wind Engineering and Industrial Aerodynamics*, 13(1-3), 313-326.

35 Tieleman, H.W. (2003). Wind tunnel simulation of wind loading on low-rise structures: a review. *Journal of Wind Engineering and Industrial Aerodynamics*, 91(12), 1627-1649.

36 Mooneghi, M. A., Irwin, P., & Chowdhury, A. G. (2016). Partial turbulence simulation method for predicting peak wind loads on small structures and building appurtenances. *Journal of Wind Engineering and Industrial Aerodynamics*, 157, 47-62.

37 Cook, N. J., & Mayne, J. R. "A refined working approach to the assessment of wind loads for equivalent static design." *Journal of Wind Engineering and Industrial Aerodynamics*, vol. 6, no. 1-2, 1980, pp. 125-137.

38 He, S., Prempain, E., and Wu, Q. H. "An improved particle swarm optimizer for mechanical design optimization problems." *Engineering Optimization*, vol. 36, no. 5, 2004, pp. 585-605.

39 Banks, A., Vincent, J., and Anyakoha, C., "A review of particle swarm optimization. Part II: hybridisation, combinatorial, multicriteria and constrained optimization, and indicative applications," *Natural Computing*, vol. 7, no. 1, 2008, pp. 109-124.